analytical chemistry

Article

pubs.acs.org/ac

Multiplexed Homogeneous Assays of Proteolytic Activity Using a Smartphone and Quantum Dots

Eleonora Petryayeva and W. Russ Algar*

Department of Chemistry, University of British Columbia, 2036 Main Mall, Vancouver, British Columbia V6T 1Z1, Canada

Supporting Information

ABSTRACT: Semiconductor quantum dot (QD) bioconjugates, with their unique and highly advantageous physicochemical and optical properties, have been extensively utilized as probes for bioanalysis and continue to generate widespread interest for these applications. An important consideration for expanding the utility of QDs and making their use routine is to make assays with QDs more accessible for laboratories that do not specialize in nanomaterials. Here, we show that digital color imaging of QD photoluminescence (PL) with a smartphone camera is a viable, easily accessible readout platform for quantitative, multiplexed, and real-time bioanalyses. Red-, green-, and blue-emitting CdSeS/ZnS QDs were conjugated with peptides that were labeled with a deep-red fluorescent dye, Alexa Fluor 647, and the dark quenchers, QSY9 and QSY35, respectively, to generate Förster resonance energy transfer (FRET) pairs sensitive to proteolytic activity. Changes in QD PL caused by the activity of picomolar to nanomolar concentrations of protease were detected as changes in the red-green-blue (RGB) channel intensities in digital color images. Importantly, measurements of replicate samples made with smartphone imaging and a sophisticated fluorescence plate reader yielded the same quantitative results, including initial proteolytic rates and specificity constants. Homogeneous two-plex and three-plex assays for the activity of trypsin, chymotrypsin, and enterokinase were demonstrated with RGB imaging. Given the ubiquity of smartphones, this work largely removes any instrumental impediments to the adoption of QDs as routine tools for bioanalysis in research laboratories and is a critical step toward the use of QDs for point-of-care diagnostics. This work also adds to the growing utility of smartphones in analytical methods by enabling multiplexed fluorimetric assays within a single sample volume and across multiple samples in parallel.

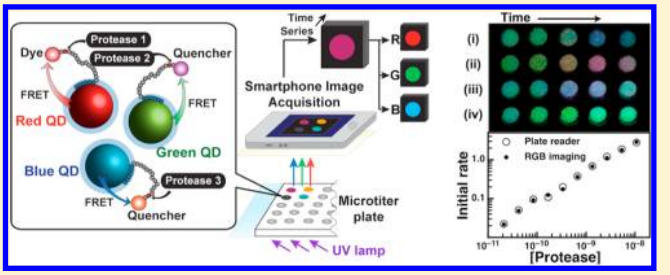

Semiconductor quantum dots (QDs) are one of many promising nanomaterials for bioanalytical applications.[1−4] Their cumulatively unique properties include, but are not limited to, size- and composition-tunable photoluminescence (PL), broad absorption spectra with large molar absorption coefficients, and an inorganic interface that can be chemically derivatized and conjugated with biomolecules.[1,2] QDs can therefore act as scaffolds for the assembly of bioprobes and biosensors and have been widely utilized for multiplexed assays and multicolor imaging, where their spectrally narrow PL and the ability to excite many colors of QD at a common wavelength are highly advantageous.[3,4] Many of these applications utilize Förster resonance energy transfer (FRET) for the detection of biological targets such as nucleic acids,[5] metal ions,[6] drugs,[7] nitric oxide,[8] and antigens,[9] as well as the activity of proteases,[10] kinases,[11] and nucleases.[12] The optical properties of QDs are ideal for FRET, permitting optimization of spectral overlap integrals and FRET efficiencies while minimizing crosstalk and background signals. Increases and decreases in FRET efficiency can be coupled to biorecognition events to generate "turn off" and "turn on" sensing depending on the design. Such configurations have been the topic of several detailed reviews.[13,14]

Despite the capabilities and growing popularity of QDs, there are still impediments to their broader utilization in laboratories that do not specialize in nanomaterials. That is, laboratories in which researchers want to use QDs in a "kit"-like fashion for bioanalyses, but the QD itself is not a focus of the research. One impediment is the availability of biofunctional QD materials, which is being addressed through growing commercial availability, as well as refined synthetic, derivatization, and bioconjugation methods that are both simpler and greener.[15−17] Another impediment to the broader utilization of QDs is the availability of instrumentation that can fully access the advantages of QDs, such as in optical multiplexing. For example, many laboratories may not have convenient access to fluorimetric equipment that can operate with excitation at ultraviolet/blue wavelengths and offer spectral acquisition or suitable filter-based color channels across the visible spectrum, particularly when real-time detection is desired. In such cases, there is no reason to switch from assay methods that are compatible with existing equipment, even if a multiplexed assay with QDs would be advantageous in principle. There is a clear need for analytical methods that can take full advantage of the optical properties of QDs and which have a minimal barrier for

Received: January 12, 2014
Accepted: February 17, 2014

   dx.doi.org/10.1021/ac500131r | *Anal. Chem.* XXXX, XXX, XXX−XXX

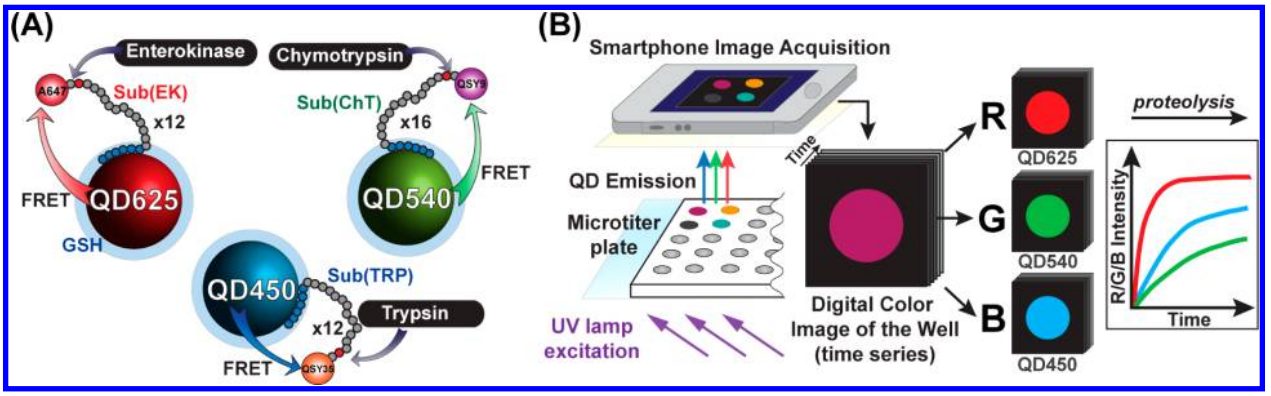

Figure 1. (A) Design of a homogeneous multiplexed assay to monitor protease activity *via* FRET with QD donors. Acceptor (QSY35, QSY9, or A647)-labeled peptide substrates containing a cleavage site for trypsin (TRP), chymotrypsin (ChT), or enterokinase (EK) were assembled on QDs with blue (QD450), green (QD540), and red (QD625) emission. The numbers in the abbreviations for the QDs indicate the approximate wavelength of their emission maximum. (B) Protease activity was measured through the recovery of QD PL and the resulting increase in the corresponding RGB channel intensity in digital color images acquired with a smartphone and a hand-held UV lamp for excitation.

Table 1. Peptide Substrate Sequences

amino acid sequence (written N-terminal to C-terminal)[a]	abbreviation	QD donor
HHHHHH SP_6S GQGEGEGNSG**R**↓GGSGNG C(QSY35)	Sub(TRP1)-QSY35	QD450
HHHHHH SP_6G SDGNESGLVP**R**↓GSG C(A647)	Sub(TRP2)-A647	QD625
HHHHHH SP_6S GQGEGEGNSAA**Y**↓ASGNG C(QSY9)	Sub(ChT)-QSY9	QD540
HHHHHH SP_6S GQGEGGNS**DDDDK**↓SGNG C(A647)	Sub(EK)-A647	QD625

[a]Protease recognition sites are indicated in bold, and the hydrolysis position is indicated by the downward arrow.

adoption in laboratories that have little or no prior experience with QDs or limited instrumentation available. Importantly, methods that can achieve this goal are also a critical step toward adapting QD-based bioanalyses for point-of-care (POC) diagnostics.

To address the above challenges, we have combined the spectrally narrow PL emission and strong, broad light absorption of QDs with red-green-blue (RGB) digital color imaging for quantitative, multiplexed homogeneous assays. A smartphone camera, which is ubiquitous in modern society, was used as the imaging platform, and multiplexed homogeneous assays of proteolytic activity were demonstrated as proof-of-concept. As shown in Figure 1, alloyed CdSeS/ZnS QDs with emission in the blue, green, and red region of the spectrum were each conjugated with a dye-labeled peptide substrate containing a recognition site that was hydrolyzed by one of three proteases (trypsin, chymotrypsin, or enterokinase). The dye labels were selected to be acceptors for the QDs, quenching their PL *via* FRET. In the absence of protease activity, the FRET acceptors remained in close proximity to their QDs, leading to efficient energy transfer. Proteolysis of the peptide substrates released the acceptor dyes from the QD and restored QD PL. Analogous FRET-based probes for sensing proteolytic activity have been reported previously[10,18−20] but have required spectrofluorimeters, fluorescence plate readers, or fluorescence microscopes for readout. Most of these proteolytic assays have also been nonmultiplexed. Here, we show that quantitative, real-time detection of proteolytic activity is possible using a readout platform as simple and as accessible as a smartphone camera and a hand-held UV lamp (i.e., black light), where changes in QD PL were measured from RGB channel intensities in digital color images. The smartphone readout was first validated by comparison to assays done with a fluorescence plate reader; then, multiplexed smartphone assays were demonstrated, including a homogeneous three-plex assay of proteolytic activity with QDs. The results show that the unique optical properties of QDs can be combined with FRET and signal readout from smartphone camera images for multiplexed, quantitative bioanalyses that are feasible in almost any laboratory.

EXPERIMENTAL SECTION

Detailed experimental methods can be found in the Supporting Information.

Materials. Alloyed CdSeS/ZnS core/shell QDs (CytoDiagnostics, Burlington, ON, Canada) with PL emission maxima at 450, 525, 540, and 625 nm (abbreviated QD450, QD525, QD540, and QD625, respectively) were made water-soluble by coating with glutathione (GSH) ligands. Peptides (Bio Synthesis Inc., Lewisville, TX) were labeled with QSY35-iodoacetamide, QSY9-maleimide, or Alexa Fluor 647 (A647)-maleimide (Life Technologies, Carlsbad, CA) as described previously (see Supporting Information for details).[21] The peptide sequences are shown in Table 1 and are designed to be substrates for either trypsin (TRP), chymotrypsin (ChT), or enterokinase (EK), with almost no cross-reactivity.[22] The peptides were terminated with a hexahistidine sequence to permit spontaneous, high-affinity ($K_d \sim 10^{-9}$ M) self-assembly to the QDs.[23,24] QD−peptide conjugates were prepared by mixing the desired number of moles of QDs and peptides together, at the desired ratio, in the desired volume of buffer (see Supporting Information, Table S1).

Enzyme Assays. For protease assays, samples of QD−peptide conjugates were individually prepared with QD−peptide ratios of 1:12, 1:16, and 1:12 for QD450, QD540, and QD625, respectively, using the dye-labeled peptides specified in Table 1. Peptide conjugates of QD450 (100 pmol), QD540 (20 pmol), and/or QD625 (30 pmol) were mixed in a final volume of 50 μL of borate buffer (10 mM, pH 8.4, 50 mM NaCl). Solutions of trypsin (TRP; 21 pM−32 nM), chymotrypsin

dx.doi.org/10.1021/ac500131r | Anal. Chem. XXXX, XXX, XXX−XXX

Table 2. Properties of the QDs and FRET Pairs Used for RGB Imaging[a]

channel	QD PL (nm)	QY	BX	GX	RX	acceptor	R_0 (nm)
blue (B)	450	0.032	–	<0.1%	<1%	QSY35	3.5
green (G)	540	0.16	9%	–	<0.1%	QSY9	4.7
red (R)	625	0.10	7%	6%	–	A647	5.3

[a]QY = QD donor quantum yield; X = crosstalk; B = blue channel; G = green channel; R = red channel; R_0 = Förster distance.

(ChT; 20 pM–40 nM), and/or enterokinase (EK; 1–9 nM) were prepared at twice the desired concentration, and 50 μL of the protease solution was added to the QD–peptide conjugates. Color images were acquired at 20 s intervals for 1 h. Protease activity was quantified from the initial rates of hydrolysis, measured as the slope of the initial linear region of progress curves (see Supporting Information for details).

PL Measurements and Image Acquisition. QDs were excited using a hand-held (6 W) or portable, battery-powered (4 W) UV lamp with emission at 365 nm (UVP, Upland, CA, USA). Images were acquired using an iPhone 4S (Apple, Cupertino, CA, USA) with the iLapse software application (MEA Mobile Ltd., New Haven, CT, USA) for automated image acquisition. Images were then processed using ImageJ (NIH, Bethesda, MD) with the Time Series Analyzer v2.0 plug-in. A long-pass filter (400 nm cutoff) and a short-pass filter (650 nm cutoff) were placed in front of the camera lens to block excitation light and any A647 emission, respectively. PL spectra were acquired with a Tecan Infinite M1000 plate reader (Tecan Ltd., Morrisville, NC, USA). A detailed description of the data analysis methods is included in the Supporting Information.

RESULTS

RGB Color Imaging of Quantum Dots. Digital cameras produce color images using a built-in Bayer mosaic filter (or similar) placed over CCD or CMOS detectors, where color images are interpolated from 2 × 2 arrays of physical pixel elements with overlaid red, green, and blue (RGB) filters.[25] The wavelength ranges are estimated to be 360–510 nm, 500–600 nm, and 560–700 nm for the blue, green, and red channels, respectively. To test the suitability of the Bayer filter pattern for imaging multiple colors of QDs, samples of QDs with emission maxima within the transmission range of each RGB channel (QD625, QD525 or QD540, and QD450) were added to the clear-bottomed wells of a microtiter plate, obliquely trans-illuminated with a hand-held UV lamp, and RGB color images acquired using a smartphone camera. The relative crosstalk between the RGB channels for QD450, QD540, and QD625 is summarized in Table 2, and the corresponding images are shown in the Supporting Information (Figure S1). Compared to the QD540, the QD525 had more than triple the crosstalk in the blue channel, making the QD540 the better choice as the green emitter. The relationship between the color channel intensity (measured with the smartphone camera) and the integrated QD PL intensity (measured with a fluorescence plate reader) is shown in Figure 2A for increasing concentrations of QD450, QD540, and QD625. The observed trends were approximately linear over short intervals but exhibited some curvature as the upper limit of the RGB channel intensity was approached (R, G, B = 255). The red channel was the most sensitive and retained good linearity at low PL intensities. In contrast, the green and blue channels exhibited sharp decreases in sensitivity at low PL intensities. These observations defined the working range for assays.

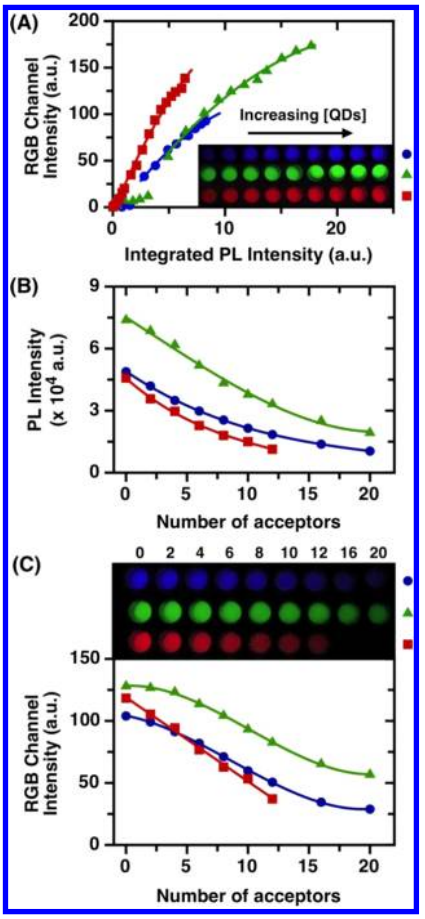

Figure 2. (A) Color images of various concentrations of QDs (inset) and the correlation between the measured RGB channel intensities and the integrated PL intensities for QD450 (blue ●), QD540 (green ▲), and QD625 (red ■). (B) Calibration curves showing the decrease in QD PL intensity as the number of acceptors per QD increases for QD450–[Sub(TRP1)-QSY35] (blue ●), QD540–[Sub(ChT)-QSY9] (green ▲), and QD625–[Sub(TRP2)-A647] (red ■) conjugates. (C) Calibration curves for the same samples as in panel B, showing decreases in RGB channel intensities as the number of acceptors per QD increases. The inset shows smartphone images of the samples in microtiter plate wells. See Supporting Information for an explanation of the shadows in the images.

FRET Pairs and Their Fidelity. The three FRET pairs used in this work were QD450–QSY35, QD540–QSY9, and QD625–A647 (written as donor–acceptor). The absorption and emission spectra for each QD and each dye are shown in the Supporting Information (Figure S3). The dark quenchers, QSY35 and QSY9, were paired with QD450 and QD540 to maximize the multiplexing capacity of the homogeneous assay within the visible spectrum. Use of a fluorescent dye acceptor would have introduced broad FRET-sensitized emission, causing significant crosstalk in other color channels (e.g., a fluorescent acceptor for the QD540 would have had emission

dx.doi.org/10.1021/ac500131r | Anal. Chem. XXXX, XXX, XXX–XXX

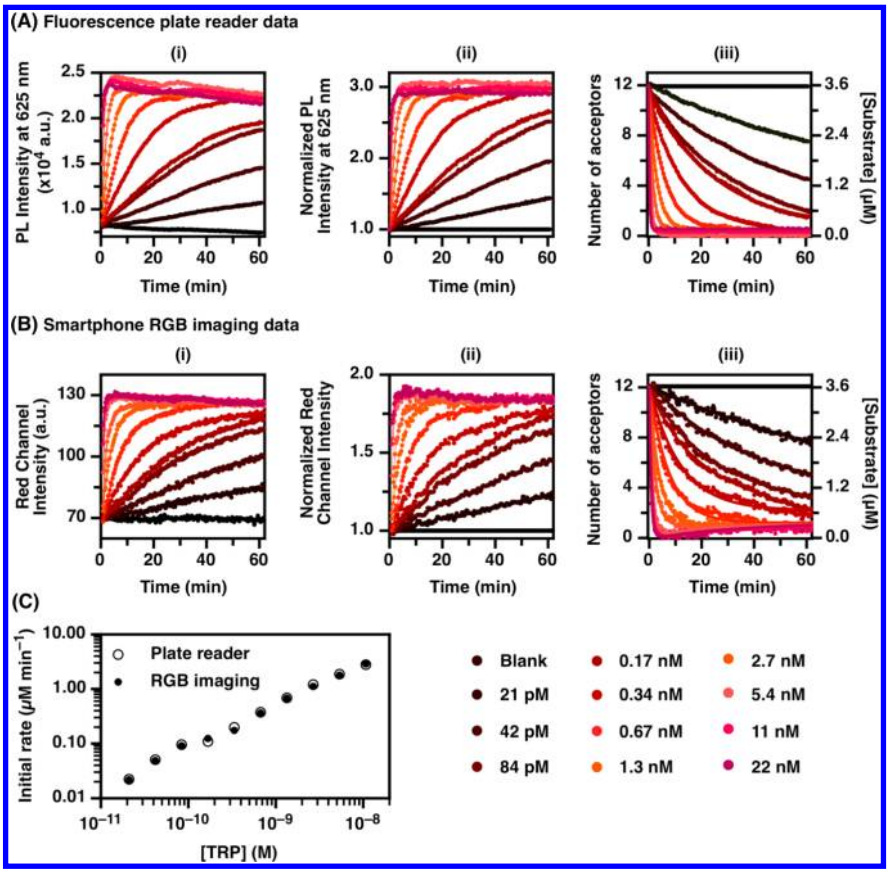

Figure 3. Proteolytic digestion of QD625−$[Sub(TRP2)-A647]_{12}$ conjugates by TRP and comparison of data acquired with (A) a fluorescence plate reader and (B) a smartphone and RGB imaging: (i) raw PL data; (ii) normalized PL data; (iii) conversion of the normalized PL data to the average number of acceptors per QD and the bulk equivalent concentration of peptide substrate. (C) Comparison of initial proteolytic rates measured from the fluorescence plate reader data and smartphone RGB imaging data.

in the red channel, which was used to measure QD625 PL). A647 was used as the acceptor for the QD625 because it provided a large Förster distance and because its FRET-sensitized emission was easily blocked with a short-pass filter. The Förster distances for the FRET pairs are given in Table 2, and the spectral overlap integrals and other pertinent photophysical parameters are listed in the Supporting Information (Table S2). One of the advantages of using QDs as FRET donors is that energy transfer efficiencies can be incrementally improved by the progressive assembly of more acceptor-labeled peptides per QD. Figure 2B shows changes in QD PL intensity, measured with a fluorescence plate reader, as a function of the number of acceptor-labeled peptides per QD. Figure 2C shows the same calibration curves but instead plots the RGB color channel intensities measured from smartphone camera images. The QD PL and RGB channel intensities decreased as the number of acceptors increased. FRET efficiencies (see Supporting Information, Figure S4) were calculated from QD PL quenching and reached 77% for QD450−QSY35 (20 peptides), 73% for QD540−QSY9 (20 peptides), and 74% for QD625−A647 (12 peptides).

It should be noted that the final concentration of QD450 was 1.00 μM in all experiments (cf. 0.20 μM for QD540 and 0.30 μM for QD625) to achieve signal intensities in the blue channel that were comparable to those in the green and red channels of color images. This concentration was necessitated by the lower quantum yield of the QD450 (see Table 2). Although it was possible to acquire smartphone images of QDs down to concentrations as low as 10−50 nM by adjusting the excitation intensity from the UV lamp (i.e., proximity to the microtiter plate), a minimum QD concentration of 0.20 μM was used to ensure complete assembly with the labeled peptides. The coordination of the hexahistidine-terminated peptides to QDs is an equilibrium process governed by $K_d \approx 10^{-9}$ M and the overall concentrations of peptide and QD.[23,24] The fidelity of the unique QD−FRET pair probes prepared for multiplexed assays depended on the off-rate (k_{off}) for the assembled peptides being slow relative to the duration of the assay. To confirm the stability of the prepared QD−peptide conjugates, RGB channel intensities were tracked over 1 h in the presence and absence of other QDs. Less than 4% increases in RGB channel intensities (see Supporting Information, Table S3) were observed for QD donors in mixtures with unconjugated QDs (cf. >150% change during proteolysis), suggesting that there was minimal dissociation of peptides from QDs. The fidelity of the initial peptide assembly was further confirmed by tracking mobility shifts between QDs and QD−peptide conjugates on an agarose gel, where a QD−peptide conjugate in a mixture retained an electrophoretic mobility that was lower than the nonconjugated QDs and consistent with that measured for the conjugate alone (see Supporting Information, Figure S5).

Validation of Proteolytic Assays with Digital Color Imaging. The ability to track protease activity using RGB digital images was first tested in a one-color format. QD450−$[Sub(TRP1)-QSY35]_{12}$, QD540−$[Sub(ChT)-QSY9]_{16}$, and

dx.doi.org/10.1021/ac500131r | Anal. Chem. XXXX, XXX, XXX−XXX

QD625−[Sub(TRP2)-A647]$_{12}$ conjugates were exposed to various concentrations of either TRP or ChT. In each case, the number of peptides per QD was chosen so that there would be an approximately linear increase in the corresponding RGB channel intensity as the number of acceptors per QD decreased with proteolysis (see Figure 2C). Samples dispensed into the wells of a microtiter plate were illuminated with a UV lamp, and digital color images were acquired with a smartphone. A blank sample (i.e., no enzyme) was measured in parallel and used as a reference to account for drift in the UV lamp intensity (see Supporting Information, Figure S6) and potential photobrightening or photobleaching of the QDs.[26] The response of the smartphone camera was relatively constant with estimated RGB channel intensity fluctuations <0.6% (see Supporting Information, Figure S7).

Figure 3 shows representative data for the activity of TRP with QD625−[Sub(TRP2)-A647]$_{12}$ conjugates, where changes in QD625 PL were monitored in the red channel of digital images. Increases in protease concentration increased the rate of peptide digestion, resulting in faster increases in the red channel intensity. For data analysis, the measured red channel intensities of the acquired images were normalized to unity at the initial time point, thereby accounting for small variations in excitation intensity between different wells of the microtiter plate and between different experiments. To validate the smartphone imaging readout, proteolytic activity in replicate samples was measured with a fluorescence plate reader in parallel. For quantitative analysis of proteolysis kinetics, the relative QD PL signals were converted into the number of substrate peptides per QD at each time point in an assay by comparison to calibration curves (see Supporting Information, Figure S8). These calibration curves needed to account for the nonspecific adsorption of digested peptide on the QDs, and we therefore prepared mixed digest/substrate calibration curves as described previously.[27,28] Importantly, this calibration was also able to account for decreases (up to 18%) in QD PL intensity upon the assembly of peptides to the QDs (see Supporting Information, Figure S9). Initial rates of digestion were determined from the initial slope of the progress curves (see Supporting Information for details) and plotted as a function of protease concentration to determine the apparent specificity constant, k_{cat}/K_m (see Supporting Information for details). Although proteolysis at the interface of nanoparticles does not necessarily follow standard Michaelis−Menten kinetics,[27] this parameter was useful for comparing the data between the smartphone and fluorescence plate reader detection formats. As listed in Table 3, similar values of k_{cat}/K_m were obtained from both the smartphone and plate reader formats, indicating good quantitative agreement between the two methods. A paired t test comparison of the initial rates measured with the smartphone and plate reader readout formats indicated that the null hypothesis could not be rejected at any reasonable level of confidence (p = 0.47 across all TRP concentrations, where p is the probability that the observed variation will occur if the null hypothesis is true).

Table 3. Comparison of the Specificity Constants, k_{cat}/K_m (M^{-1} s^{-1}), Calculated for One-Plex Assays between the Fluorescent Plate Reader and Smartphone RGB Imaging Readout Formats

readout format	QD450/TRP	QD540/ChT	QD625/TRP
plate reader	1.2×10^5	4.9×10^5	2.2×10^6
smartphone	1.4×10^5	5.0×10^5	2.0×10^6

Similar proteolytic assays were done with QD540−[Sub-(ChT)-QSY9]$_{16}$ and QD450−[Sub(TRP1)-QSY35]$_{12}$ conjugates using both smartphone digital imaging and the fluorescence plate reader (see Supporting Information, Figures S10 and S11). Again, the progress curves generated from the smartphone imaging and plate reader measurements were qualitatively similar and, in a statistical comparison of the initial rates, the null hypothesis could not be rejected at a reasonable level of confidence (p = 0.21 or 0.30 for QD540 across all ChT concentrations or [ChT] > 0.6 nM, respectively; p = 0.68 for QD450 across all TRP concentrations). As shown in Table 3, there was also good agreement between the calculated specificity constants. Overall, the utility of the smartphone readout format for quantitative measurements of protease activity was confirmed by the close correlation between the data generated with a fluorescence plate reader and the data generated *via* RGB imaging.

Multiplexed Proteolytic Assays with Digital Color Imaging. We next evaluated the two-plex detection of TRP and ChT using the smartphone imaging readout. Mixtures of QD450−[Sub(TRP1)-QSY35]$_{12}$ and QD540−[Sub(ChT)-QSY9]$_{16}$, or QD625−[Sub(TRP2)-A647]$_{12}$ and QD540−[Sub(ChT)-QSY9]$_{16}$, were exposed to different concentrations of TRP and ChT. Progress curves for three different combinations of ChT and TRP are shown in Figure 4. Representative raw data is shown in the Supporting Information (Figure S12). Analogous to the one-plex assays, the rates of change in the RGB channel intensities were proportional to the concentrations of the corresponding proteases. Interestingly, small decreases in the initial rates of digestion were observed in two-plex assays relative to one-plex assays with QD625−[Sub(TRP2)-A647]$_{12}$ (30 pmol) and QD540−[Sub(ChT)-QSY9]$_{16}$ (20 pmol), and a significant decrease was observed for ChT activity in the system containing the QD450−[Sub(TRP1)-QSY35]$_{12}$ (100 pmol) and QD540−[Sub(ChT)-QSY9]$_{16}$ (20 pmol) conjugates. This effect was observed with both the smartphone imaging and the fluorescence plate reader detection formats. Nontrivial interactions between proteases (or other proteins) and nanoparticle interfaces have been reported previously.[27,29,30] These results suggest that protease activity can be influenced by the total concentration of QDs in a sample and not just the concentration of the QDs carrying the substrate of interest. Our group is currently studying such interactions between QDs and proteases, but we limit our focus here to the smartphone readout strategy, which gave results analogous to the fluorescence plate reader. Another interesting observation in two-plex assays was that the increased optical density of QD mixtures decreased the overall signal intensities relative to samples with only one color of QD, in both the RGB imaging and plate reader formats (see Supporting Information, Figure S2). Quantitative multiplexed assays should therefore be calibrated as mixtures.

To demonstrate three-plex assays, a series of samples containing QD450−[Sub(TRP1)-QSY35]$_{12}$ (100 pmol), QD540−[Sub(ChT)-QSY9]$_{16}$ (20 pmol), and QD625−[Sub-(EK)-A647]$_{12}$ (30 pmol) were exposed to various concentrations of TRP, ChT, and EK. Mixtures were interrogated in microtiter plates using UV lamp illumination and smartphone digital imaging. Figure 5 shows progress curves and a time series of RGB color images obtained with three different

dx.doi.org/10.1021/ac500131r | Anal. Chem. XXXX, XXX, XXX−XXX

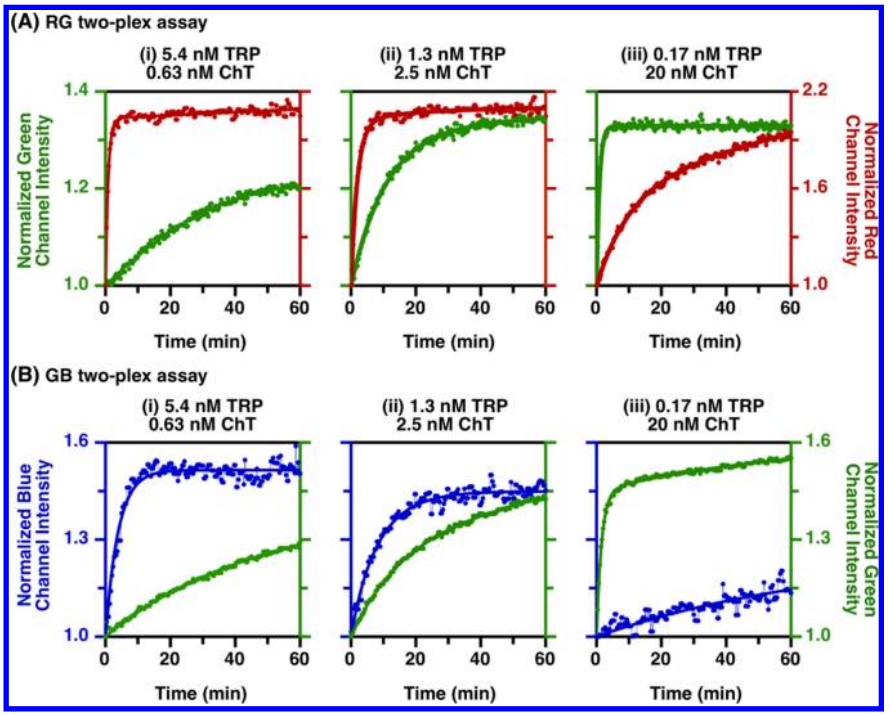

Figure 4. Progress curves for two-plex homogeneous assays of proteolytic activity. (A) RG two-plex assay with QD540−[Sub(ChT)-QSY9]$_{16}$ (20 pmol) and QD625−[Sub(TRP2)-A647]$_{12}$ (30 pmol). (B) GB two-plex assay with QD450−[Sub(TRP1)-QSY35]$_{12}$ (100 pmol) and QD540−[Sub(ChT)-QSY9]$_{16}$ (20 pmol). The conjugates were exposed to the indicated mixtures of TRP and ChT. The ordinate and abscissa scales are the same in each panel of (A) or (B).

mixtures of TRP, ChT, and EK. Consistent with the expectations, increases in the concentration of one of the proteases in the mixture correlated with more rapid changes in the RGB channel intensity for the corresponding color of QD. The normalized initial rates of digestion of QD450−[Sub(TRP1)-QSY35]$_{12}$ conjugates by TRP were in relatively good agreement with those in the one-plex assay; however, ChT activity in the three-plex assays decreased by *ca.* 50% in comparison to the one-plex assay, suggesting that there may be stronger nonproteolytic interactions between QDs and ChT than between QDs and TRP. Nonetheless, the rates of change in the RGB channel intensities in each three-plex assay were proportional to the concentration of the corresponding target protease.

DISCUSSION

The foregoing experiments have clearly demonstrated that RGB imaging of QD PL with a smartphone camera is suitable for quantitative, real-time, *in vitro* bioanalysis. Although we used a kinetic assay format to demonstrate the full capability of the method, single-point measurements are also possible. Suitable assay times may range from 10 min to upward of 1 h with longer times providing lower limits of detection. A kinetic analysis using initial rates offers a larger dynamic range. Proteolytic assays were an excellent model system because QD−FRET probes for protease activity are well-known[20,31] and because assays of proteolytic activity have diagnostic and therapeutic value. Abnormal protease activity is associated with various diseases, including cancer,[32] neurodegenerative diseases,[33] and arthritis,[34] among many others. Protease inhibitors are also an important class of drugs.[35] The apparent effect of QD concentration on proteolytic rates is a biophysical phenomenon that remains to be further elucidated, but this effect is independent of the analytical readout platform, and QD-based assays of activity and inhibition remain possible. We expect that this smartphone readout methodology will be compatible with many other QD−FRET assays reported in the literature, including hybridization assays,[5] carbohydrate assays,[36] and immunoassays.[37,38] The methodology should also be compatible with charge transfer-based quenching assays with QDs.[39,40]

There is a growing body of literature on the use of smartphones as detectors in various analytical methods. In particular, smartphones have been suggested to be amenable to POC diagnostics and telemedicine.[41] Compared to traditional analytical instruments, smartphones are more portable, have lower cost, and have an inherent capacity for data storage, data processing, and data sharing/retrieval. Smartphones are also ubiquitous, with an estimated 56% of American and Canadian adults owning one in 2013.[42,43] Martinez et al. were among the first to suggest the use of a smartphone camera for quantitative analysis of colorimetric assays.[41] More recently, Wei et al. used a diode laser and smartphone camera to image single fluorescent dye-doped polystyrene nanoparticles and dye-labeled virus particles.[44] Gallegos et al. used a smartphone camera in combination with a diffraction grating as a transducer for light transmission in bioassays on photonic crystal chips,[45] and Ayas et al. integrated a smartphone camera into a confocal Raman system to measure single molecules on plasmonic substrates.[46] Our work here adds to this literature, introducing for the first time the possibility of a homogeneous multiplexed analysis of a single sample volume through the unique PL properties of QDs and the color channels of a smartphone camera. In parallel, our method also provides for the simultaneous analysis of many samples in an array format through imaging. These capabilities are achieved with minimal expense, without custom or complex instrumentation, and would not have been feasible without QDs. Tunable, spectrally

dx.doi.org/10.1021/ac500131r | *Anal. Chem.* XXXX, XXX, XXX−XXX

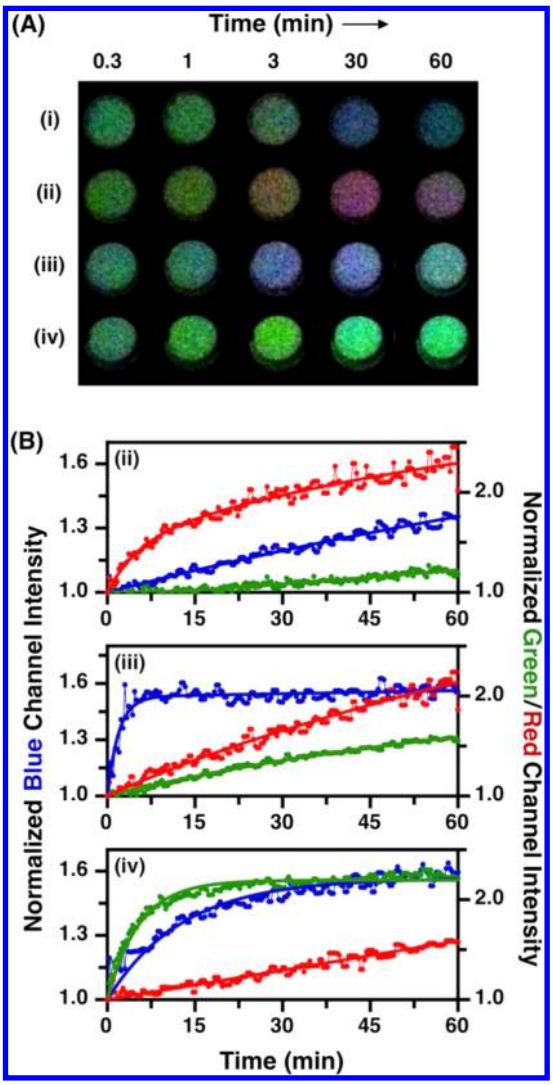

Figure 5. Three-plex homogeneous proteolytic assays. (A) Representative color images (brightness enhanced for clarity; see Supporting Information, Figure S13, for raw image) for QD450–[Sub(TRP1)-QSY35]$_{12}$ (100 pmol), QD540–[Sub(ChT)-QSY9]$_{16}$ (20 pmol), and QD625–[Sub(EK)-A647]$_{12}$ (30 pmol) mixed with various concentrations of TRP, ChT, and EK: (i) reference sample (no proteases); (ii) 1 nM TRP, 1 nM ChT, and 4.5 nM EK; (iii) 8.6 nM TRP, 2 nM ChT, and 1.5 nM EK; (iv) 2.2 nM TRP, 16 nM ChT, and 0.5 nM EK. (B) Progress curves corresponding to (ii), (iii), and (iv).

narrow PL was needed to match the Bayer color filter channels of the smartphone camera, and a large effective Stokes shift was necessary to permit rejection of excitation light with simple optical filters. Moreover, the bright QD PL was needed to provide sufficient sensitivity.

Our work here is significant because it makes QDs a more accessible research tool for all laboratories and because it further suggests that smartphone imaging, particularly with QD probes, has long-term potential for POC diagnostics. In this vein, we have previously shown that emission from QD525–Alexa Fluor 555 FRET pairs immobilized on a paper substrate can be used for quantitative analysis of proteolytic activity using an R/G ratio and smartphone color digital imaging.[22] This format was heterogeneous and relied on a spatial array format for multiplexing. The current homogeneous format with spectral multiplexing is similarly promising for POC applications but is more versatile and better suited for laboratory research. Our previous work also demonstrated that three different camera devices gave analogous results.[22] We therefore expect that different models of smartphones can be used for assays similar to those described here with an iPhone.

CONCLUSIONS

We have shown that the combination of QDs, FRET, and imaging with a smartphone is a viable, easily accessible platform for quantitative, real-time bioanalyses. The optical properties of QDs also enhance the general utility of smartphone cameras as detectors in analytical methods, particularly in terms of multiplexing. Homogeneous assays of proteolytic activity were used as model systems for proof-of-concept, where a deep-red fluorescent dye and dark quencher labels on peptides were FRET acceptors for red-, green-, and blue-emitting QD donors. Changes in the PL emission from these QDs were detected in the RGB color channels of digital color images and could be correlated to the activity of picomolar to nanomolar concentrations of protease. Importantly, RGB imaging with a smartphone yielded the same quantitative results as replicate assays done with a sophisticated fluorescence plate reader. In addition to assays with a single color of QD, homogeneous two-plex and three-plex assays for the activity of TRP, ChT, and EK were also demonstrated. We expect that the methods and data analysis presented here can be extended to a wide range of established QD–FRET bioanalyses for targets other than proteases. Given the ubiquity of smartphones, this work largely removes any instrumental impediments to the adoption of QDs as routine bioanalytical tools in laboratories that do not specialize in luminescent nanomaterials. Additionally, this work represents an important preliminary step toward POC diagnostics based on QDs.

ASSOCIATED CONTENT

Supporting Information

Detailed experimental methods including materials, instrumentation, data acquisition and analysis, additional results including analysis of crosstalk and QD mixtures, PL spectra and spectral overlap, tests of QD–peptide conjugate stability, additional results for RGB readout in one-plex assays, and representative non-normalized data for multiplexed smartphone camera assays. This material is available free of charge via the Internet at http://pubs.acs.org.

AUTHOR INFORMATION

Corresponding Author

*E-mail: algar@chem.ubc.ca.

Notes

The authors declare no competing financial interest.

ACKNOWLEDGMENTS

E.P. is grateful to the Natural Sciences and Engineering Research Council of Canada (NSERC) for a postgraduate scholarship. The authors thank the University of British Columbia, the Canada Foundation for Innovation (CFI), and NSERC for financial support of this research. W.R.A. is also grateful for a Canada Research Chair (Tier 2).

REFERENCES

(1) Mattoussi, H.; Palui, G.; Na, H. B. *Adv. Drug Delivery Rev.* **2012**, *64*, 138–166.

(2) Zrazhevskiy, P.; Sena, M.; Gao, X. H. *Chem. Soc. Rev.* **2010**, *39*, 4326−4354.
(3) Petryayeva, E.; Algar, W. R.; Medintz, I. L. *Appl. Spectrosc.* **2013**, *67*, 215−252.
(4) Jin, Z.; Hildebrandt, N. *Trends Biotechnol.* **2012**, *30*, 394−403.
(5) Freeman, R.; Liu, X.; Willner, I. *Nano Lett.* **2011**, *11*, 4456−4461.
(6) Wu, C. S.; Oo, M. K. K.; Fan, X. *ACS Nano* **2010**, *4*, 5897−5904.
(7) Zhang, C. Y.; Johnson, L. W. *Anal. Chem.* **2009**, *81*, 3051−3055.
(8) Wang, S.; Han, M. Y.; Huang, D. *J. Am. Chem. Soc.* **2009**, *131*, 11692−11694.
(9) Wegner, K. D.; Jin, Z.; Lindén, S.; Jennings, T. L.; Hildebrandt, N. *ACS Nano* **2013**, *7*, 7411−7419.
(10) Medintz, I. L.; Clapp, A. R.; Brunel, F. M.; Tiefenbrunn, T.; Uyeda, H. T.; Chang, E. L.; Deschamps, J. R.; Dawson, P. E.; Mattoussi, H. *Nat. Mater.* **2006**, *5*, 581−589.
(11) Freeman, R.; Finder, T.; Gill, R.; Willner, I. *Nano Lett.* **2010**, *10*, 2192−2196.
(12) Huang, S.; Xiao, Q.; He, Z. K.; Liu, Y.; Tinnefeld, P.; Su, X. R. *Chem. Commun.* **2008**, 5990−5992.
(13) Algar, W. R.; Tavares, A. J.; Krull, U. J. *Anal. Chim. Acta* **2010**, *673*, 1−25.
(14) Medintz, I. L.; Mattoussi, H. *Phys. Chem. Chem. Phys.* **2009**, *11*, 17−45.
(15) Yong, K. T.; Law, W. C.; Roy, I.; Ling, Z.; Huang, H. J.; Swihart, M. T.; Prasad, P. N. *J. Biophotonics* **2011**, *4*, 9−20.
(16) Palui, G.; Avellini, T.; Zhan, N. Q.; Pan, F.; Gray, D.; Alabugin, I.; Mattoussi, H. *J. Am. Chem. Soc.* **2012**, *134*, 16370−16378.
(17) Jennings, T. L.; Becker-Catania, S. G.; Triulzi, R. C.; Tao, G. L.; Scott, B.; Sapsford, K. E.; Spindel, S.; Oh, E.; Jain, V.; Delehanty, J. B.; Prasuhn, D. E.; Boeneman, K.; Algar, W. R.; Medintz, I. L. *ACS Nano* **2011**, *5*, 5579−5593.
(18) Chang, E.; Miller, J. S.; Sun, J.; Yu, W. W.; Colvin, V. L.; Drezek, R.; West, J. L. *Biochem. Biophys. Res. Commun.* **2005**, *334*, 1317−1321.
(19) Shi, L. F.; De Paoli, V.; Rosenzweig, N.; Rosenzweig, Z. *J. Am. Chem. Soc.* **2006**, *128*, 10378−10379.
(20) Kim, G. B.; Kim, Y. P. *Theranostics* **2012**, *2*, 127−138.
(21) Sapsford, K. E.; Farrell, D.; Sun, S.; Rasooly, A.; Mattoussi, H.; Medintz, I. L. *Sens. Actuators, B* **2009**, *139*, 13−21.
(22) Petryayeva, E.; Algar, W. R. *Anal. Chem.* **2013**, *85*, 8817−8825.
(23) Aldeek, F.; Safi, M.; Zhan, N. Q.; Palui, G.; Mattoussi, H. *ACS Nano* **2013**, *7*, 10197−10210.
(24) Sapsford, K. E.; Pons, T.; Medintz, I. L.; Higashiya, S.; Brunel, F. M.; Dawson, P. E.; Mattoussi, H. *J. Phys. Chem. C* **2007**, *111*, 11528−11538.
(25) Spring, K. R. *Meth. Cell Biol.* **2007**, *81*, 171−187.
(26) Lee, S. F.; Osborne, M. A. *Chem. Phys. Chem.* **2009**, *10*, 2174−2191.
(27) Algar, W. R.; Malanoski, A.; Deschamps, J. R.; Blanco-Canosa, J. B.; Susumu, K.; Stewart, M. H.; Johnson, B. J.; Dawson, P. E.; Medintz, I. L. *Nano Lett.* **2012**, *12*, 3793−3802.
(28) Algar, W. R.; Malanoski, A. P.; Susumu, K.; Stewart, M. H.; Hildebrandt, N.; Medintz, I. L. *Anal. Chem.* **2012**, *84*, 10136−10146.
(29) You, C. C.; De, M.; Rotello, V. M. *Curr. Opin. Chem. Biol.* **2005**, *9*, 639−646.
(30) Lynch, I.; Dawson, K. A. *Nano Today* **2008**, *3*, 40−47.
(31) Knudsen, B. R.; Jepsen, M. L.; Ho, Y. P. *Expert Rev. Mol. Diagn.* **2013**, *13*, 367−375.
(32) Folgueras, A. R.; Pendas, A. M.; Sanchez, L. M.; López-Otín, C. *Int. J. Dev. Biol.* **2004**, *48*, 411−424.
(33) Rosenberg, G. A. *Lancet Neurol.* **2009**, *8*, 205−216.
(34) Yasuda, Y.; Kaleta, J.; Bromme, D. *Adv. Drug Delivery Rev.* **2005**, *57*, 973−993.
(35) Scott, C. J.; Taggart, C. C. *Biochimie* **2010**, *92*, 1681−1688.
(36) Freeman, R.; Bahshi, L.; Finder, T.; Gill, R.; Willner, I. *Chem. Commun.* **2009**, 764−766.
(37) Kattke, M. D.; Gao, E. J.; Sapsford, K. E.; Stephenson, L. D.; Kumar, A. *Sensors* **2011**, *11*, 6396−6410.
(38) Chen, L.; Zhang, X.; Zhou, G.; Xiang, X.; Ji, X.; Zheng, Z.; He, Z.; Wang, H. *Anal. Chem.* **2012**, *84*, 3200−3207.
(39) Medintz, I. L.; Pons, T.; Trammell, S. A.; Grimes, A. F.; English, D. S.; Blanco-Canosa, J. B.; Dawson, P. E.; Mattoussi, H. *J. Am. Chem. Soc.* **2008**, *130*, 16745−16756.
(40) Sandros, M. G.; Shete, V.; Benson, D. E. *Analyst* **2006**, *131*, 229−235.
(41) Martinez, A. W.; Phillips, S. T.; Carrilho, E.; Thomas, S. W.; Sindi, H.; Whitesides, G. M. *Anal. Chem.* **2008**, *80*, 3699−3707.
(42) Oliveira, M. Smartphone addiction grows in Canada: Google survey. In *The Globe and Mail's Report on Business*; Phillip Crawley: Toronto, July 29, 2013.
(43) Smith, A. *Smartphone Ownership 2013*; Pew Research Center's Internet & American Life Project: Washington, D.C., USA, June 5, 2013.
(44) Wei, Q.; Qi, H.; Luo, W.; Tseng, D.; Ki, S. J.; Wan, Z.; Göröcs, Z.; Bentolila, L. A.; Wu, T. T.; Sun, R.; Ozcan, A. *ACS Nano* **2013**, *7*, 9147−9155.
(45) Gallegos, D.; Long, K. D.; Yu, H.; Clark, P. P.; Lin, Y.; George, S.; Nath, P.; Cunningham, B. T. *Lab Chip* **2013**, *13*, 2124−2132.
(46) Ayas, S.; Cupallari, A.; Ekiz, O. O.; Kaya, Y.; Dana, A. *ACS Photonics* **2014**, *1*, 17−26.